6th International Conference on Earthquake Geotechnical Engineering
1-4 November 2015
Christchurch, New Zealand

Two-Dimensional Site Effects for Dry Granular Soils

D. Asimaki[1] and S. Jeong[2]

ABSTRACT

We present a parametric numerical study on site amplification triggered by step-like slopes of dry granular soils overlaying bedrock. We specifically show that the inelastic soil response and the presence of a strong soil-bedrock impedance contrast, can each significantly affect the intensity and frequency of ground motions near the slope crest. This finding suggests that incomplete site characterization that lacks information about the deeper geologic formations can lead to underestimation of 2D site effects, which include 1D site response, topographic amplification, and their coupling in the layers above the soil-rock interface. Our results also show that the vertical component of ground motion near the crest, which is generated purely from diffraction and mode conversion of vertically propagating shear waves, can have very high amplitude, sometimes higher than the horizontal component at the same station. The effects of such high vertical ground motions and their spatial variability on nearby structures require further study.

Introduction

The modification of seismic ground motion near topographic features, known as topography effects, has been long acknowledged and extensively studied. Previous studies (Boore 1972; Sanchez-Sesma 1985; Geli et al. 1988) have shown that earthquake ground motions can be significantly amplified due to the interference of incident, diffracted and mode-converted waves caused by irregular surface topographies. These studies, however, have been based on assumptions of homogeneous linear elastic soils and simplified surface geometries (Geli et al. 1988). More recently, however, research has shown that topography effects can be significantly affected by the stratigraphy and dynamic response characteristics of soil layering (Assimaki et al. 2005; Grazier 2009): a stratified soil with irregular surface geometry subjected to vertically incident shear waves can yield very different amplification pattern from the same geometry on homogeneous soil. To differentiate between the various phenomena, we shall refer to the modification of ground motion by the surface geometry as *topography effects*, and to the combined effects of topography and layering as *site effects*.

The complexity of site effects has been recognized by previous studies that often reported notable discrepancy between predictive models of topography effects and field observations. Recently, Dafni (2013) tested the seismic response of step-like slopes at the NEES@UCDavis centrifuge facility, to investigate whether nonlinear soil behavior, which is ignored by most predictive models of topography effects, could partially explain this discrepancy. To supplement Dafni's study, we performed detailed parametric numerical simulations in which we further investigated the role of nonlinear soil behavior, as well as the combined effects of ground geometry and soil stratigraphy in shaping the ground surface motion.

[1]Professor, Department of Mechanical and Civil Engineering, California Institute of Technology, Pasadena, USA, domniki@caltech.edu
[2]Postdoctoral Fellow, Department of Civil and Natural Resources Engineering, University of Canterbury, Christchurch, New Zealand, seokho.jeong@canterbury.ac.nz

Numerical Model and Soil Constitutive Parameters

To validate our numerical model, we simulated the dynamic response of the centrifuge physical model using a 2.5D finite element model (plane strain with equivalent off-plane stiffness of the 3D model) using the computer code DYNAFLOW^{TM} (Prevost 1995). Figure 1 shows the finite element mesh of the 30 degree slope model and the locations of accelerometers used for comparison of our simulations to the experiments.

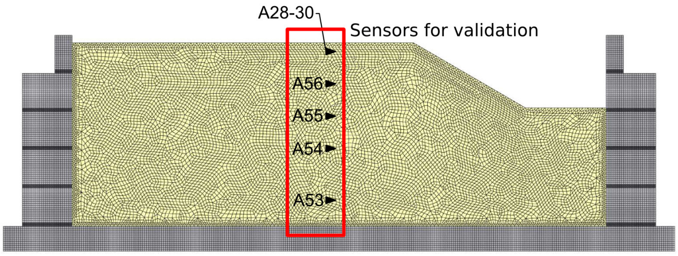

Figure 1: Finite element mesh and locations of accelerometers used for the comparison of simulations and experiments.

The physical model was constructed using dry Nevada sand with a target relative density, DR = 100 %; the dynamic response characteristics of dense Nevada sand are well documented in the experimental study by Stevens et al. (1999). In our model, the pressure dependency of the elastic modulus was approximated by the following power law equation:

$$G = G_0 \left(\frac{p}{p_0}\right)^n \tag{1}$$

Figure 2a shows the shear wave velocity profile of Nevada sand with DR = 100 % measured by Stevens et al. (1999), who used low strain signals generated by an air hammer attached to the centrifuge container base plate. However, experimental results of Dafni (2013) suggested that the shear wave velocity of the physical model test shown in Figure 2a was lower than the result of Stevens et al. (1999), perhaps because the target DR was not quite achieved. We thus used a velocity profile with the functional form suggested by Stevens et al, but calibrated to match the 1D site response of Dafni's experiments. This profile is also shown in Figure 2a.

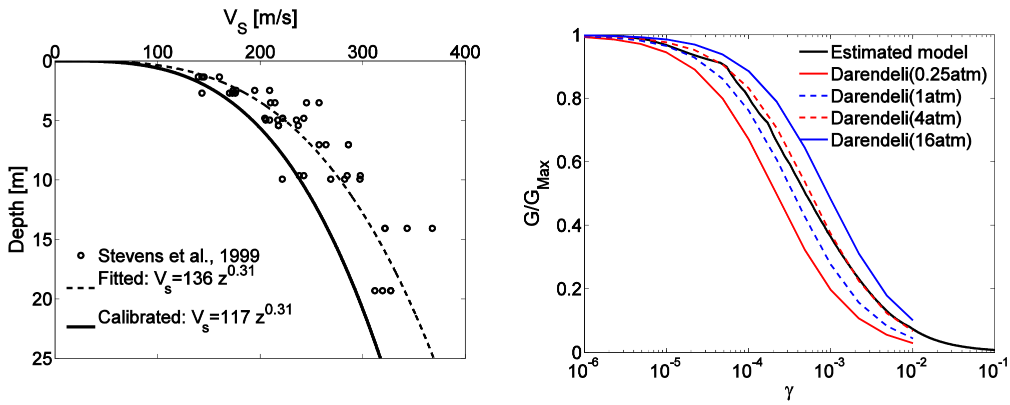

Figure 2: (a) Pressure dependency of the shear wave velocity; (b) Estimated modulus reduction curve.

To simulate the hysteretic response of Nevada sand, we employed the pressure dependent multi yield (PDMY) plasticity model by Prevost (1985), with a purely kinematic hardening rule and round-cornered Mohr-Coulomb yield surfaces. We simulated the monotonic shear stress-strain soil response using the generalized hyperbolic model by Hayashi et al. (1994). Figure 2b shows the corresponding backbone curve at the reference pressure p_{ref} = 100 kPa, compared to the widely employed modulus reduction curves by Darendeli (2001). Table 1 summarizes the soil constitutive parameters used in our simulations.

Table 1: Material parameters calibrated for dry Nevada sand with relative density D_R=100 %.

Density, ρ [Mg/m3]	**Poisson's ratio, ν**	**Initial shear modulus, G_0 [MPa]**	**Reference pressure, p_{ref} [kPa]**	**Friction angle, ϕ [degree]**
1.7	0.25	108	100	42

Numerical Model Validation

We next compared the simulated motions to the experimental data at the vertical array of accelerometers marked by the red box in Figure 1. Figure 3 shows examples of simulated accelerations at the surface behind the slope crest (A28-30 in Figure 1), compared to experiments in time and frequency domain. Simulated and recorded motions show excellent agreement for various input motions both in time and frequency domain. Accelerations recorded at A28-30 show small variations, which validates the assumption of plane strain condition at the center of the physical model. Figure 4 shows the comparison of acceleration time histories along the vertical array of accelerometers (A29, A56, A55, A54 and A53 in Figure 1).

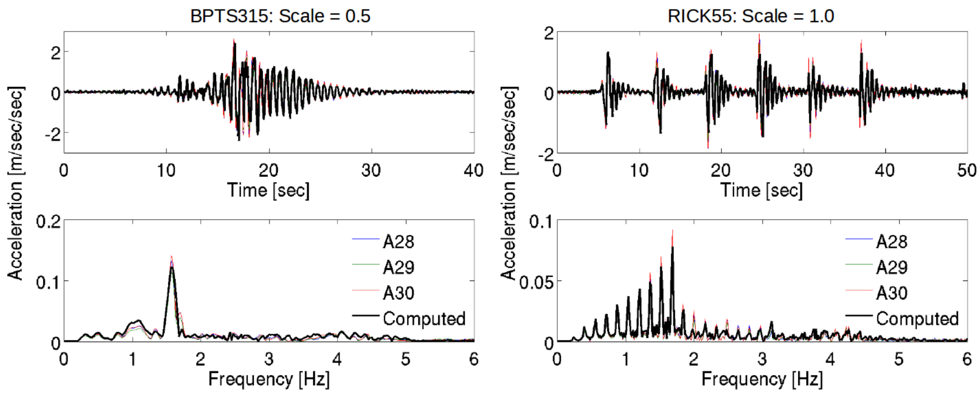

Figure 3: Comparison of simulation and experiments at sensors A28-30.

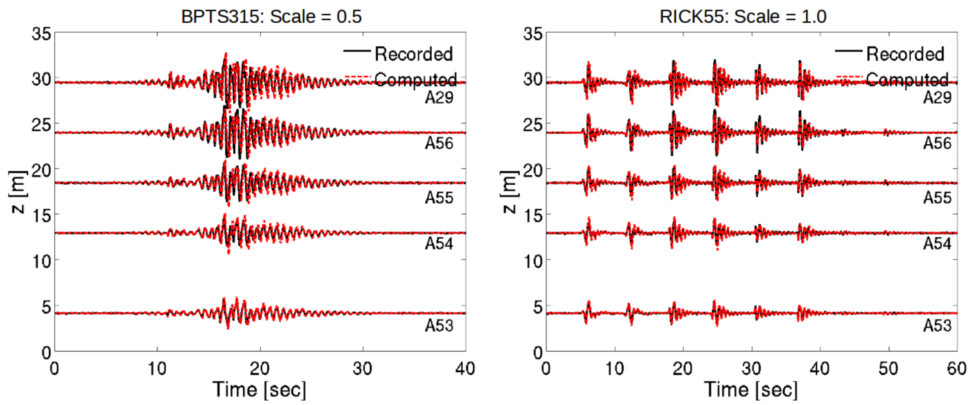

Figure 4: Comparison of simulation and experiments along the vertical array of sensors.

Numerical Model for Parametric Analyses

Despite the effectiveness of the laminar box to approximate far-field conditions, the mismatch between container and soil flexibility unavoidably gave rise to reflections that contaminated the direct effects of topography near the crest (Jeong et al. 2015). To isolate site effects from boundary effects, we next removed the laminar box elements of the computational domain and extended the numerical model laterally to approximately 6 times the size of the centrifuge model. Figure 5 shows the extended model used for the parametric analyses. Lateral boundaries of the extended model were treated with free-field boundary conditions to minimize the spurious reflections from the artificial boundaries. The absorbing boundary condition at the base of the model is treated with Lysmer dashpots (Lysmer & Kuhlemeyer 1969), and the input motions are prescribed with equivalent nodal forces at the base and sides of the model. For more information, we refer the reader to Jeong et al. (2015).

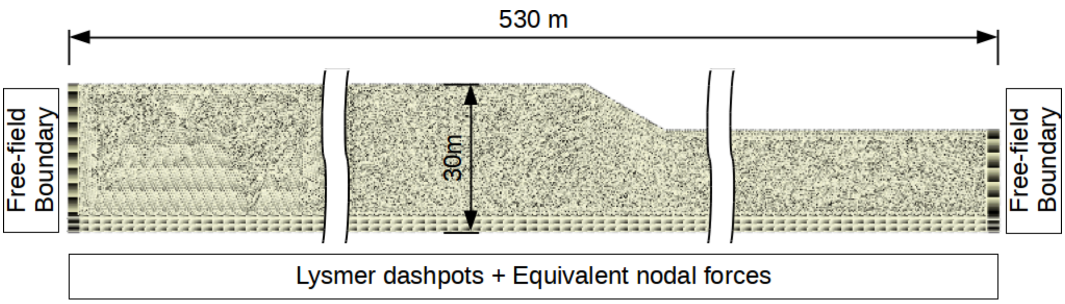

Figure 5: Finite element mesh, and boundary conditions of the extended model used for parametric studies.

In the parametric study that follows, we used a train of Ricker wavelets as input motion, applied at the base of the model as equivalent nodal forces. The input motion shown in Figure 6 consists of three Ricker wavelets, with central frequencies of f_0 = 1.8, 7 and 20 Hz, to ensure it covers a wide band of frequencies (see frequency spectrum on the right). A low intensity motion was used initially, with peak incident velocity of 0.003 m/s (shear stress, τ = 1.7 kPa), to study the small strain (i.e. nearly elastic) response of the slope. We next used a series of increasingly intense ground motions, to investigate the role of nonlinear soil response.

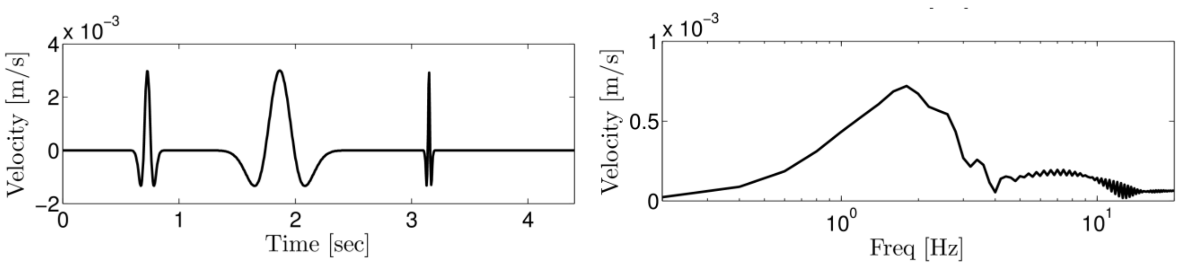

Figure 6: The time history and Fourier spectra of the input motion applied at the base of the model as equivalent nodal forces.

Slope Height as Frequency-Dependent Scaling Parameter

Previous studies (Ashford et al. 1997; Bouckovalas & Papadimitriou 2005) have shown that for homogeneous soil conditions, the topographic frequencies are inversely proportional to the height of the slope. We first tested whether this finding holds for the case of smoothly varying velocity profiles such as these of granular media. In the following analysis, the slope height will be presented in dimensionless form, normalized by the wavelength that corresponds to the central frequency of the Ricker pulse and the average velocity of the soil column behind the slope.

We considered three different slope heights: h = 5.5 m, 11 m and 22 m, namely one equal to the original model height (h = 11 m) and two scaled versions of the original model. The velocity profile was unchanged for all three model configurations; thus, the average shear wave velocities over the height of the slope were V_S = 190, 234 and 289 m/s, respectively. Figure 7 shows the horizontal and vertical spectral ratios—defined as the response at the crest normalized by horizontal one-dimensional far-field response— and plotted as function of the dimensionless frequency, $f \times h/V_S$. Our results showed that the slope height is an effective scaling parameter that can capture the frequency-dependency of topography effects not only for homogeneous soils, but also for layered soils with smoothly varying velocity.

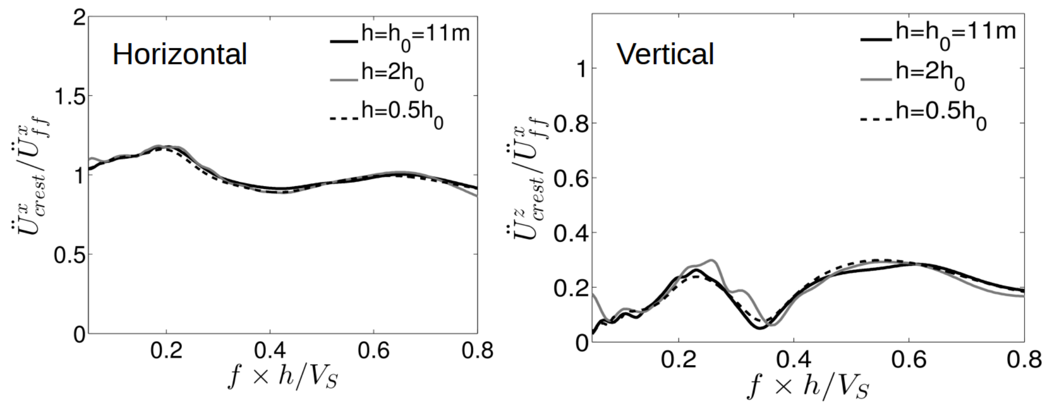

Figure 7: Effect of the slope height. Scaling is valid when the size factor is the only variable.

Near-Surface Impedance Contrast: Low Velocity Layer

Irregular topographies are often covered by relatively thin and soft surficial soils or weathered rock. However, the interactions between the topography and the soil/rock stratigraphy are poorly understood, and the coupling between site and topographic amplification has only been studied for isolated case studies (Assimaki et al. 2005; Assimaki & Jeong 2013; Paolucci et al. 1999). We investigated the effects of the low velocity layer near the surface behind the slope crest on the intensity of topographic amplification. We specifically conducted simulations with two soft soil thicknesses t = 4m and 8m, and 3 different impedance contrasts, α = 1.5, 2 and 3. The impedance contrast at the interface is defined as $\alpha = \rho_l V_{sl} / \rho_u V_{su}$, where ρ_l and V_{sl} are the density and the shear wave velocity of lower layer, and ρ_u and V_{su} are the density and the shear wave velocity of upper layer, respectively. Figure 8 summarizes the velocity profiles considered.

Results depicted in Figure 9 show that the increase in impedance contrast drastically changes both the amplitude and frequency content of the spectral ratios of ground motion behind the crest. Specifically, the maximum amplification of both horizontal and vertical components increased monotonically with increasing impedance contrast; and the number of peaks and troughs of the ground motion frequency spectrum behind the crest increased as well. Results also showed very intensified vertical accelerations, reaching 60% and 90% of the far-field

(1D conditions) horizontal components for impedance contrasts α = 2 and 3, respectively.

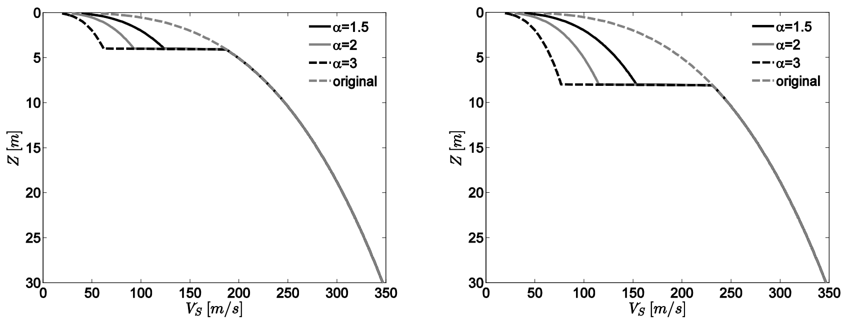

Figure 8: Shear wave velocity profiles behind the crest of the slopes studied.

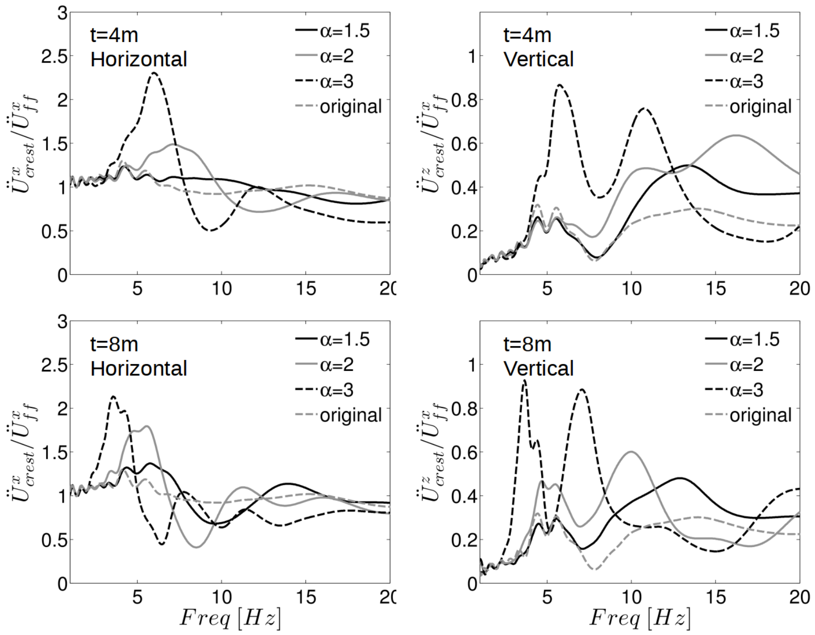

Figure 9: Effect of surficial low velocity zone.

Impedance Contrast at Depth: Elastic Bedrock

Centrifuge experimental results by Dafni (2013) showed conspicuous amplifications at 3.5 Hz and 6.5Hz. In a companion study, we recently showed that the high amplification observed during the experiments was caused by reverberating waves trapped in the soil layer above the aluminum base plate, which acted as semi-rigid bedrock that prevented radiation damping. This finding suggested that topographic amplification could be strongly affected by the presence of a deep soil-bedrock impedance contrast (Jeong et al. 2015). To demonstrate the effect of bedrock on topographic amplifications, we introduced a bedrock layer at the base of our numerical model with impedance contrast α_B = 1.5, 2 and 3 relative to the soil.

Figure 10 summarizes the effects of bedrock on topographic amplification for the scenarios considered. Results suggest that the presence of bedrock can significantly increase the crest-far-field spectral ratios amplitude. For the model considered, the amplitude of the vertical component was even more sensitive to the soil-bedrock impedance contrast. Amplification factors increased monotonically with increasing soil-bedrock impedance contrasts, while there wasn't any significant change in the frequency components that experienced amplification. This is very important because it differentiates the vertical component caused by direct shear wave diffraction from the P-wave velocity, whose frequency content is often too high to cause infrastructure damage.

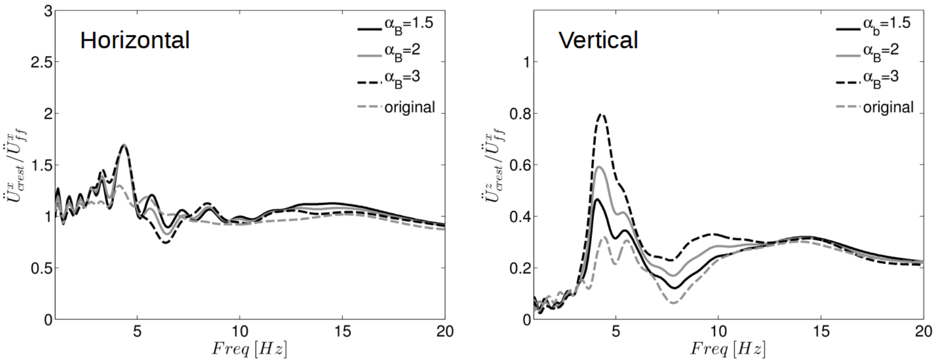

Figure 10: Effect of soil-bedrock impedance contrast.

Effects of the Nonlinear Soil Response

So far we focused on the low strain response of the slope. To demonstrate the effect of soil nonlinearity on topographic amplification, we next conducted simulations with input motions of increased intensities. The input velocity time histories were scaled to 0.003, 0.01, 0.04, 0.08 and 0.1 m/s (τ^{i}_{max} = 1.7, 5.6, 22.4, 44.9, 56.1 kPa). Figure 11 demonstrates the effect of increasing peak input velocity on the crest-far-field spectral ratios, using the original velocity profile that didn't show prominent amplification with low-intensity input. Our results showed significantly increased amplification factors for peak incident velocities higher than 0.04 m/s. Also, the vertical components were more sensitive to the soil nonlinearity, especially for the higher frequencies. At f = 15 Hz, the vertical acceleration exceeded the amplitude of the free-field horizontal acceleration for peak incident velocities higher than 0.08 m/s.

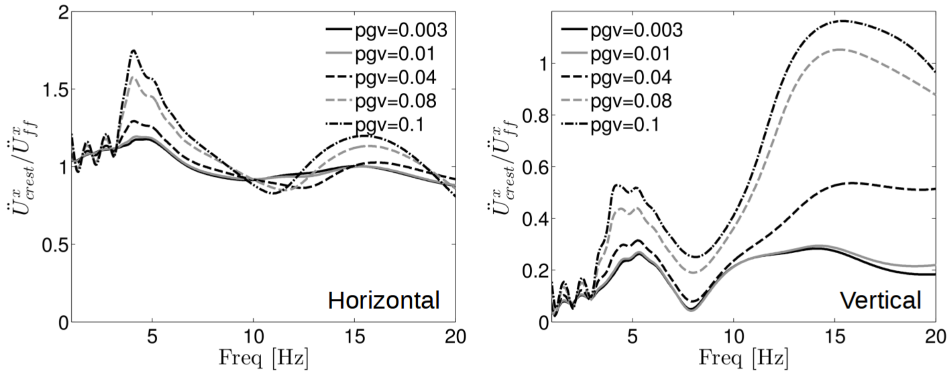

Figure 11: Effect of input motion intensity on the amplification of ground motions at the slope crest.

Conclusions

We presented a detailed parametric study on the effects of the slope height, stratigraphy, and soil-nonlinearity on the amplification of ground motions at the crest of a 30 degree singlefaced slope, using a plane strain finite element model validated with centrifuge experiments. Our results demonstrated that the soil/rock stratigraphy significantly affects the topographic amplification. Overall, sharper velocity contrasts resulted in higher amplifications, which suggests that incomplete 1D site characterization may lead to underestimation of 2D site effects.

Simulations with input motions of various intensities showed that the inelastic response of pressure-dependent soils near the surface has a unique impact on the amplification intensity and frequency characteristics of topographic amplification, which could differ substantially from the viscoelastic model predictions traditionally used in studies of such effects. We also observed that the vertical component of ground motion near the crest that is generated purely from diffraction and mode conversion of horizontally polarized incident waves can have very high amplitude, sometimes higher than the horizontal component at the same station. The effects of such high vertical ground motions and their spatial variability on nearby structures require further study.

Acknowledgments

Partial support for this research has been provided by the National Science Foundation under grant awards CMMI-0936543, CMMI-1132373 and CMMI-0619078. This support is gratefully acknowledged.

References

Ashford, S.A. et al., 1997. Topographic effects on the seismic response of steep slopes. *Bulletin of the seismological Society of America*, **87**(3), pp.701–709.

Assimaki, D. & Jeong, S., 2013. Ground Motion Observations at Hotel Montana during the M 7.0 2010 Haiti Earthquake: Topography or Soil Amplification? *Bulletin of Seismological Society of America*, **103**(5), pp.2577–2590.

Assimaki, D., Kausel, E. & Gazetas, G., 2005. Soil-dependent topographic effects: A case study from the 1999 Athens earthquake. *Earthquake Spectra*, **21**(4), pp.929–966.

Boore, D.M., 1972. A note on the effect of simple topography on seismic SH waves. *Bulletin of the seismological Society of America*, **62**(1), pp.275–284.

Bouckovalas, G.D. & Papadimitriou, A.G., 2005. Numerical evaluation of slope topography effects on seismic ground motion. *Soil Dynamics and Earthquake Engineering*, **25**(7-10), pp.547–558.

Dafni, J., 2013. *Topographic Modifications of Ground Motion and the Initiation of Coseismic Landslides*. University of Washington.

Darendeli, M.B., 2001. *Development of a new family of normalized modulus reduction and material damping curves*. University of Texas at Austin.

Geli, L., Bard, P.-Y. & Jullien, B., 1988. The effect of topography on earthquake ground motion: A review and new results. *Bulletin of the Seismological Society of America*, **78**(1), pp.42–63.

Grazier, V., 2009. Low-velocity zone and topography as a source of site amplification effect on Tarzana hill, California. *Soil Dynamics and Earthquake Engineering*, **29**(2), pp.324–332.

Hayashi, H. et al., 1994. Modeling of nonlinear stress strain relations of sands for dynamic response analysis. In *Tenth World Conference on Earthquake Engineering*. Balkema.

Jeong, S. et al., 2015. Virtual centrifuge experiments on topography effects. *Soil Dynamics and Earthquake Engineering*.

Lysmer, J. & Kuhlemeyer, R.L., 1969. Finite Dynamic Model For Infinite Media. *Journal of the Engineering Mechanics Division*, **95**(4), pp.859–878.

Paolucci, R., Faccioli, E. & Maggio, F., 1999. 3D Response analysis of an instrumented hill at Matsuzaki, Japan, by a spectral method. *Journal of Seismology*, **3**, pp.191–209.

Prevost, J.H., 1985. A simple plasticity theory for frictional cohesionless soils. *Soil Dynamics and Earthquake Engineering*, **4(**1), pp.9–17.

Prevost, J.H., 1995. *DYNAFLOW: A nonlinear transient finite element analysis program*,

Sanchez-Sesma, F.J., 1985. Diffraction of elastic SH waves by wedges. *Bulletin of the Seismological Society of America*, **75**(5), pp.1435–1446.

Stevens, D.K. et al., 1999. *Comprehensive investigation of nonlinear site response - Centrifuge data report for {DKS02}*